EVALUATING VITERBI DECODED REED-SOLOMON BLOCK CODES ON A COMPLEX SPREADED DS/SSMA CDMA SYSTEM

L. Staphorst and L.P. Linde
Department of Electrical, Electronic & Computer Engineering, University of Pretoria, Pretoria, South Africa, 0002. Email: leon.staphorst@eng.up.ac.za

Abstract: In recent years, the Viterbi Algorithm (VA) has been shown to be an efficient trellis decoder for binary and non-binary linear blocks. In this simulation study the performance of VA decoded non-binary Reed-Solomon (RS) block codes, employed in a wideband Code Division Multiple Access (CDMA) system, operating in multipath fading channel conditions, is considered. The RAKE receiver-based Direct Sequence Spread Spectrum Multiple Access (DS/SSMA) Quadrature Phase Shift Keying (QPSK) system employed in this study uses Complex Spreading Sequence (CSS), such as Zadoff-Chu (ZC), Double Sideband (DSB) Constant Envelope Linearly Interpolated Root-of-Unity (CE-LI-RU) filtered General Chirp-like (GCL), Analytical Bandlimited Complex (ABC) and Quadriphase (QPH) sequences. This paper firstly describes the notion of VA decoding of linear block codes. Background information is then given on the filtered and unfiltered CSS families employed in the simulation study. Next, the complex Direct Sequence Spread Spectrum Multiple Access (DS/SSMA) Quadrature Phase Shift Keying (QPSK) transmitter and RAKE receiver simulator structures, as well as a novel complex multipath fading channel simulator structure are presented. This is then followed by a description of this study's versatile multi-user multipath fading performance evaluation platform, which is constructed using the complex RAKE receiver-based DS/SSMA QPSK communication system and complex multipath fading channel simulator structures. Lastly, simulated Bit Error Rate (BER) performances are presented for uncoded wideband systems and wideband systems employing VA decoded non-binary RS block codes in realistic multi-user multipath fading channel conditions. The effect of Multi-User Interference (MUI), as well as that of Channel State Information (CSI) on the decoding performance of the VA are also considered.

Keywords: Complex spreading sequences, DSSS/MA, multipath fading, Reed-Solomon, Viterbi algorithm

1. INTRODUCTION

In 1974 *Bahl et al.* described a novel approach whereby trellises can be constructed for linear block codes [1]. As such, block code decoding was no longer limited to just algebraic techniques. Soft decision Maximum-Likelihood (ML) decoding of block codes using the Bahl-Cocke-Jelinek-Raviv (BCJR) algorithm [1], or variants thereof, were made possible through these trellises. Following this publication, *Wolf* showed [2] that the VA can be applied to block code trellises as an efficient soft decision ML decoder, with the added bonus of being far less complex than the BCJR algorithm. A major advantage of trellis decoding algorithms in general is that they are also capable of using CSI during decoding, resulting in improved performances when utilised in fading channel conditions [3].

The application of binary sequences in DS/SSMA systems has been exhaustively investigated since introduction of Spread Spectrum (SS). Due to the availability of potentially large sets of sequences that exhibit comparable auto-correlation and improved cross-correlation properties when compared to binary sequences, interest has started to shift towards the use of non-binary and CSSs. There are numerous advantages in using CSSs in future Beyond 3G (B3G) and 4th Generation (4G) DS/SSMA systems, including the possibility to generate Constant Envelope (CE) and Single Sideband (SSB) [4–6] transmitter output signals, etc.

This paper presents a simulation study of the performance of Viterbi decoded non-binary RS block codes in a multi-user Code Division Multiple Access (CDMA) system experiencing realistic multipath fading. Among other, the influence of CSI on the performance of the VA as a soft input ML decoder for linear block codes is investigated. The paper is structured as follows: *Section* 2 considers the application of the VA to BCJR block code trellises as an optimal ML decoder. A brief overview of the families of CSS considered in this study, namely ZC, DSB Constant Envelope Linearly Interpolated Root-of-Unity (CE-LI-RU) filtered GCL, ABC and QPH sequences, is presented in *Section* 3. This is followed in *Section* 4 by descriptions of the complex DS/SSMA QPSK transmitter and RAKE receiver simulation models. *Section* 5 describes the complex multipath fading channel simulator model employed in this study. A versatile

Copyright ©2004 IEEE: An earlier edition of this paper was first published in AFRICON '04, 15 - 17 September 2004, Gaborone, Botswana

multi-user multipath simulation platform, constructed using the RAKE receiver-based DS/SSMA QPSK communication system and complex multipath fading channel simulator, is the focus of *Section* 6. *Section* 7 presents extensive simulation results, comparing the performances of uncoded and Viterbi decoded (hard and soft decision) non-binary RS block codes in multi-user multipath fading channel conditions for the different CSS families. Several concluding remarks are given in *Section* 8.

2. THE VITERBI DECODING OF LINEAR BLOCK CODES USING BCJR TRELLISES

In principle, every linear block code has a unique trellis description. By creating a set of parallel trellis paths, one for each code word, a simple albeit inefficient trellis is fabricated. In [1] *Bahl et al.* presents an elegant approach to derive an efficient trellis structure from the linear block code's parity check matrix. The BCJR trellis construction method for a (n, k, d_{min}) linear block code with code word symbols from Galois field $GF\left(2^{\xi}\right)$, requires the code's parity check matrix, given by:

$$H = [\overline{h}_1\ \overline{h}_2\ ...\ \overline{h}_n] \tag{1}$$

In Equation (1), $\overline{h}_i$, with $i = 1, 2, ..., n$, is the ith column of the parity check matrix, containing $(n-k)$ elements from the Galois field $GF\left(2^{\xi}\right)$. The trellis construction technique is based on the fact that the ith $(n-k)$-tuple syndrome vector $\overline{s}_m^i$ [7] for the mth n-tuple valid code word vector $\overline{c}_m = \{c_{m,0}, c_{m,1}, ..., c_{m,n-1}\}$, can be calculated using the following recursion formula [1, 8]:

$$\begin{aligned} \overline{s}_m^0 &= \overline{0} \\ \overline{s}_m^i &= \overline{s}_m^{i-1} + c_{m,i-1}.\overline{h}_i \end{aligned} \tag{2}$$

where $c_{m,i}$ is the ith $GF\left(2^{\xi}\right)$ code word symbol contained in the vector $\overline{c}_m$. Note that addition and multiplication is carried out symbol-wise in $GF\left(2^{\xi}\right)$. The block code trellis, which is a compact method to represent all ϵ^k, with $\epsilon = 2^{\xi}$, code words in the code, will consist of $(n+1)$ sets of nodes (states), each set containing ϵ^{n-k} nodes. By interconnecting the nodes with branches in a topology uniquely defined by H, the block code's trellis is formed. A detailed description and examples of the BCJR trellis construction algorithm is presented in [9].

Algebraic ML decoding of an (n, k, d_{min}) linear block code, with code word symbols from $GF\left(2^{\xi}\right)$, involves the comparison of the received code word with each of the ϵ^k, with $\epsilon = 2^{\xi}$, valid code words, selecting the one which proves to be the closest as the most likely transmitted one. This process can be time consuming and complex, especially for codes where both n and k are large. Conversely, the application of the VA as ML block code decoder will result in the most likely path in the code's trellis describing the received code word to be chosen, discarding several unlikely code words along the way. Depending on the parameters n and k, this decoding approach may greatly reduce decoding time and complexity. The interested reader is referred to [9] for a detailed explanation of the block-wise VA, applied to a linear block code's trellis.

3. COMPLEX SPREADING SEQUENCES

The following subsections briefly describe filtered and unfiltered CSS families considered in this study.

3.1 Unfiltered Sequences

Zadoff-Chu Sequences: ZC CSSs is a subclass of GCL CSSs [10], which is generated and characterised as follows: Let $\overline{S}_{ZC}^q = \{S_{ZC}^q[0], S_{ZC}^q[1], ..., S_{ZC}^q[M_{seq}-1]\}$ represent the vector of chips of the qth length-M_{seq} unfiltered continuous-time ZC sequence $S_{ZC}^q(t)$. With $j = \sqrt{-1}$, the ith chip in this sequence is determined as follows [6, 11]:

$$S_{ZC}^q[i] = \begin{cases} \exp\left(j\frac{\pi.a.i^2}{M_{seq}}\right) & \text{if } M_{seq} \text{ is even} \\ \exp\left(j\frac{\pi.a.i(i+1)}{M_{seq}}\right) & \text{if } M_{seq} \text{ is odd} \end{cases} \tag{3}$$

where the sequence number a can only take on integer values relatively prime to M_{seq}. As such, the family size for length-M_{seq} ZC CSSs is calculated as follows:

$$M_{fam} = 1 + \sum_{a=2}^{M_{seq}-1} \begin{cases} 1 & \text{if } M_{seq} \bmod(a) \neq 0 \\ 0 & \text{if } M_{seq} \bmod(a) = 0 \end{cases} \tag{4}$$

Hence, the largest ZC CSS families are obtained when M_{seq} is an odd prime number. In such a case the family size is $M_{fam} = M_{seq} - 1$ [6].

Quadriphase Sequences: QPH sequences are closely related to binary sequences. A length-M_{seq} QPH sequence's chip vector $\overline{S}_{QPH}^q = \left\{S_{QPH}^q[0], S_{QPH}^q[1], ..., S_{QPH}^q[M_{seq}-1]\right\}$ is constructed using two length-M_{seq} binary sequences' chip vectors, denoted as $\overline{S}_A^q = \{S_A^q[0], S_A^q[1], ..., S_A^q[M_{seq}-1]\}$ and $\overline{S}_B^q = \{S_B^q[0], S_B^q[1], ..., S_B^q[M_{seq}-1]\}$, respectively. Calculation of the ith chip of the QPH sequence is accomplished as follows [12]:

$$S_{QPH}^q[i] = \frac{1}{2\sqrt{2}}(1+j)S_A^q[i] + \frac{1}{2\sqrt{2}}(1-j)S_B^q[i] \tag{5}$$

It follows that each chip in the QPH sequence will have a value from the complex 4-symbol alphabet $\left\{\frac{1}{\sqrt{2}} + \frac{j}{\sqrt{2}}, \frac{1}{\sqrt{2}} - \frac{j}{\sqrt{2}}, -\frac{1}{\sqrt{2}} + \frac{j}{\sqrt{2}}, -\frac{1}{\sqrt{2}} - \frac{j}{\sqrt{2}}\right\}$, if the binary sequences' chip vectors $\overline{S}_A^q$ and $\overline{S}_B^q$ have chips from the antipodal alphabet $\{-1, +1\}$. For *Alltop*-type

QPH sequences [6], the family size is given as $M_{fam} = M_{seq} - 1$, with the sequence length M_{seq} limited to prime values. Furthermore, using Gold binary sequences for $\overline{S}_A^q$ and $\overline{S}_B^q$ is a popular approach [13]. Since QPH sequences are binary in nature, it follows that their complex envelopes will not be constant.

3.2 Filtered Sequences

DSB CE-LI-RU Filtered GCL Sequences: It has been shown that ZC sequences contain all the frequencies in the range $[0, M_{fam}/T_{chip})$ [Hz], with T_{chip} the duration of a chip [13]. Thus, the bandwidth of such sequences are a function of the family size. In order to bandlimit $S_{ZC}^q(t)$ and remove its dependency on the sequence index a, a $\mathrm{mod}(2\pi)$ phase constraint can be incorporated, resulting in a *Chu* sequence's chip vector denoted as $\overline{S}_{Chu}^q = \{S_{Chu}^q[0], S_{Chu}^q[1], ..., S_{Chu}^q[M_{seq}-1]\}$ [6, 11]. The ith chip of a *Chu* sequence is determined as follows:

$$S_{Chu}^q[i] = \begin{cases} \exp\left(j\frac{a.\pi.i^2}{M_{seq}}\right) \bmod (2\pi) & \text{if } M_{seq} \text{ is even} \\ \exp\left(j\frac{a.\pi.i.(i+1)}{M_{seq}}\right) \bmod (2\pi) & \text{if } M_{seq} \text{ is odd} \end{cases} \tag{6}$$

It has been shown [6] that the bandwidth of *Chu* sequences are $1/T_{chip}$ [Hz]. DSB CE-LI-RU filtered GCL sequences are obtained by filtering $S_{Chu}^q[i]$ with a *linearly interpolating root-of-unity filter* [4, 14] in order to achieve the minimum Nyquist bandwidth of $1/(2.T_{chip})$ [Hz]. The family size of such sequences is also given by Equation (4). These sequences exhibit constant complex envelopes. This characteristic alleviates the linearity constraint on power amplifiers used in DS/SSMA systems employing such sequences. Since the instantaneous power of the transmitter output signal will be constant, the communication system engineer no longer needs to be concerned with amplifier back-off. Thus, it will be possible to more efficiently utilise non-linear or partially linear power amplifiers.

ABC Sequences: ABC sequences are generated by appropriately modifying the previously defined DSB CE-LI-RU filtered GCL sequences in order to produce an injective function, as described in [4, 5]. When used in balanced QPSK structures, ABC sequences [4, 5] exhibit analytical properties, i.e. a SSB DS/SSMA signal is obtained after modulation onto the in-phase and quadrature carriers [6]. As with ZC and DSB CE-LI-RU filtered GCL sequences, the family size of ABC CSSs is determined using Equation (4).

4. RAKE RECEIVER-BASED COMPLEX DS/SSMA QPSK COMMUNICATION SYSTEMS

In the following subsections the novel complex DS/SSMA QPSK transmitter and RAKE receiver structures employed in this study are presented.

4.1 Complex DS/SSMA QPSK Transmitter Structure and Operation

Figure 1 depicts the generic structure of the complex baseband DS/SSMA QPSK transmitter of user-q in a multi-user CDMA system [7]. Assume that the mth input to this transmitter is $\overline{c}_m^q = \{c_{m,0}^q, c_{m,1}^q, ..., c_{m,W-1}^q\}$, which is a vector containing W antipodal bits with values from the alphabet $\{1, -1\}$. As shown in Figure 1, the same data bits are used on both the I-channel and Q-channel, creating a *balanced* complex DS/SSMA QPSK transmitter structure [15–17] with length-W I-channel and Q-channel symbols stream vectors, given by:

$$\begin{aligned} \overline{c}_m^{I,q} &= \{c_{m,0}^{I,q}, c_{m,1}^{I,q}, ..., c_{m,W-1}^{I,q}\} \\ &= \{c_{m,0}^q, c_{m,1}^q, ..., c_{m,W-1}^q\} \end{aligned} \tag{7}$$

and

$$\begin{aligned} \overline{c}_m^{Q,q} &= \{c_{m,0}^{Q,q}, c_{m,1}^{Q,q}, ..., c_{m,W-1}^{Q,q}\} \\ &= \{c_{m,0}^q, c_{m,1}^q, ..., c_{m,W-1}^q\} \end{aligned} \tag{8}$$

respectively. This transmitter configuration, where the symbol and bit rates are equivalent, is frequently used in DS/SSMA QPSK systems employing filtered CSSs in order to take full advantage of the spectral characteristics of the CSS. For example, in [4, 5] such a balanced transmitter structure is employed in conjunction with ABC sequences to deliver SSB transmitter output signals.

The antipodal values contained in the I-channel and Q-channel symbol stream vectors are now pulse shaped. This is accomplished by first multiplying these symbols with appropriate pulse shaping excitation signals, i.e. impulses for pulse shaping designed for impulse transmission. Square-root Nyquist pulse shaping, designed for impulse transmission, was used in the simulations that employed unfiltered CSSs Alternatively, the simulations that made use of pre-filtered CSSs employed no additional pulse shaping.

After multiplication with the excitation signals, the I-channel and Q-channel are spread with user-q's I-channel and Q-channel spreading sequences, denoted by $S_I^q(t)$ and $S_Q^q(t)$, respectively. These spreading sequences are unique to user-q. When CSSs are employed in the CDMA system, $S_I^q(t)$ and $S_Q^q(t)$ can be the real and imaginary parts of user-q's unique CSS, respectively [15, 16]. The resultant spread I-channel and Q-channel streams are given by:

$$c_m^{I,q}(t) = \sum_{j=0}^{W-1} c_{m,j}^{I,q}.x_q^I\left(t - j.T_s\right).S_I^q(t) \tag{9}$$

and:

$$c_m^{Q,q}(t) = \sum_{j=0}^{W-1} c_{m,j}^{Q,q}.x_q^Q\left(t - j.T_s\right).S_Q^q(t) \tag{10}$$

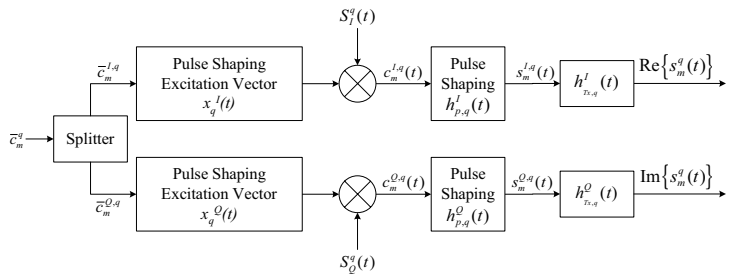

Figure 1: Complex DS/SSMA QPSK transmitter structure

respectively. In Equation (9) and Equation (10), T_s [s] is the symbol duration. The actual pulse shaping of the spread I-channel and Q-channel information are now accomplished using user-q's in-phase and quadrature pulse shaping filters, characterised by the impulse responses $h_{p,q}^I(t)$ and $h_{p,q}^Q(t)$, respectively. The resultant I-channel and Q-channel spread pulse shaped symbols are given by:

$$s_m^{I,q}(t) = c_m^{I,q}(t) \otimes h_{p,q}^I(t) \tag{11}$$

and:

$$s_m^{Q,q}(t) = c_m^{Q,q}(t) \otimes h_{p,q}^Q(t) \tag{12}$$

respectively, where $\otimes$ denotes convolution.

Lastly, the in-phase and quadrature pulse shaped symbol streams are bandlimited by the transmit filters $h_{Tx,q}^I(t)$ and $h_{Tx,q}^Q(t)$, respectively, to give user-q's complex DS/SSMA QPSK transmitter output signal:

$$s_m^q(t) = s_m^{I,q}(t) \otimes h_{Tx,q}^I(t) + j.s_m^{Q,q}(t) \otimes h_{Tx,q}^Q(t) \tag{13}$$

4.2 Complex DS/SSMA QPSK RAKE Receiver Structure and Operation

Assume that user-q's m^{th} complex DS/SSMA QPSK transmitter output signal traverses a time-invariant discrete multipath fading channel, consisting of L^q statistically independent flat faded paths. The average path gain and delay associated with this multipath channel's i^{th} path, for $i = 1, 2, ..., L^q$, are $\overline{\beta}_i^q$ and τ_i^q, respectively. Note that the complex input to user-q's receiver, denoted as $r_m^q(t)$, will consist not only of a distorted version of the signal generated by user-q's transmitter, but also disfigured signals originating from the transmitters of the other users in the CDMA system.

Figure 2 depicts the RAKE receiver structure [7], capable of optimally processing user-q's complex received signal. The first step in the demodulation process is to bandlimit the Additive White Gaussian Noise (AWGN) present in the complex received signal $r_m^q(t)$ using the I-channel lowpass receive filter $h_{Rx,q}^I(t)$ and Q-channel lowpass receive filter $h_{Rx,q}^Q(t)$. The resultant filtered complex received signal is denoted as $r_{m,filtered}^q(t)$. Next, the noisy flat faded L^q received delayed versions of user-q's m^{th} original complex transmitted signal are realigned with the last received multipath component. This is accomplished by creating L^q delayed versions of the signal $r_{m,filtered}^q(t)$, namely $r_{m,filtered}^q(t - (\hat{\tau}_{L^q}^q - \hat{\tau}_i^q))$, with $i = 1, 2, ..., L^q$. The term $\hat{\tau}_i^q$ is an estimate of the path delay of the ith multipath component. In order for the RAKE receiver to function optimally, it requires perfect knowledge of the path delay of each of the multipath components, i.e. $\hat{\tau}_i^q = \tau_i^q$ with $i = 1, 2, ..., L^q$.

Since the multipath components arriving at the receiver have experienced statistically independent flat fading and average attenuation, as dictated by the power delay profile of user-q's multipath fading channel, each received component's contribution to the total realigned m^{th} complex received signal varies. In order to increase the influence of strong multipath components and decrease the influence of weak multipath components, each of the delayed complex received signal versions is scaled, prior to demodulation, with an estimate of its average envelope amplitude. For example, the delayed filtered complex received signal $r_{m,filtered}^q(t - (\hat{\tau}_{L^q}^q - \hat{\tau}_i^q))$ is scaled by the average envelope amplitude estimate $\hat{\overline{\beta}}_i^q$. The use of this scaling technique is commonly referred to as Maximal Ratio Combining (MRC) [7, 18]. Optimal processing of the complex received signal only occurs if the receiver has perfect knowledge of the average envelope amplitude of each of the multipath components, i.e. $\hat{\overline{\beta}}_i^q = \overline{\beta}_i^q$, with $i = 1, 2, ..., L^q$.

Next, the receiver phase corrects each of the scaled and delayed versions of the mth filtered complex received signal. For the ith delayed, scaled and filtered complex received signal component $\hat{\overline{\beta}}_i^q.r_{m,filtered}^q(t - (\hat{\tau}_{L^q}^q - \hat{\tau}_i^q))$, this is accomplished by mixing it with the complex exponent $\exp\left(-j.\hat{\phi}_i^q\left(t - (\hat{\tau}_{L^q} - \hat{\tau}_i^q)\right)\right)$. The instantaneous phase $\hat{\phi}_i^q\left(t - (\hat{\tau}_{L^q} - \hat{\tau}_i^q)\right)$ is an estimate of the channel phase changes experienced by the ith complex received multipath component at the time of its reception, as well as phase distortion added by the I-channel and Q-channel receive filters. Coherent demodulation takes place in the event that the receiver has perfect knowledge of the

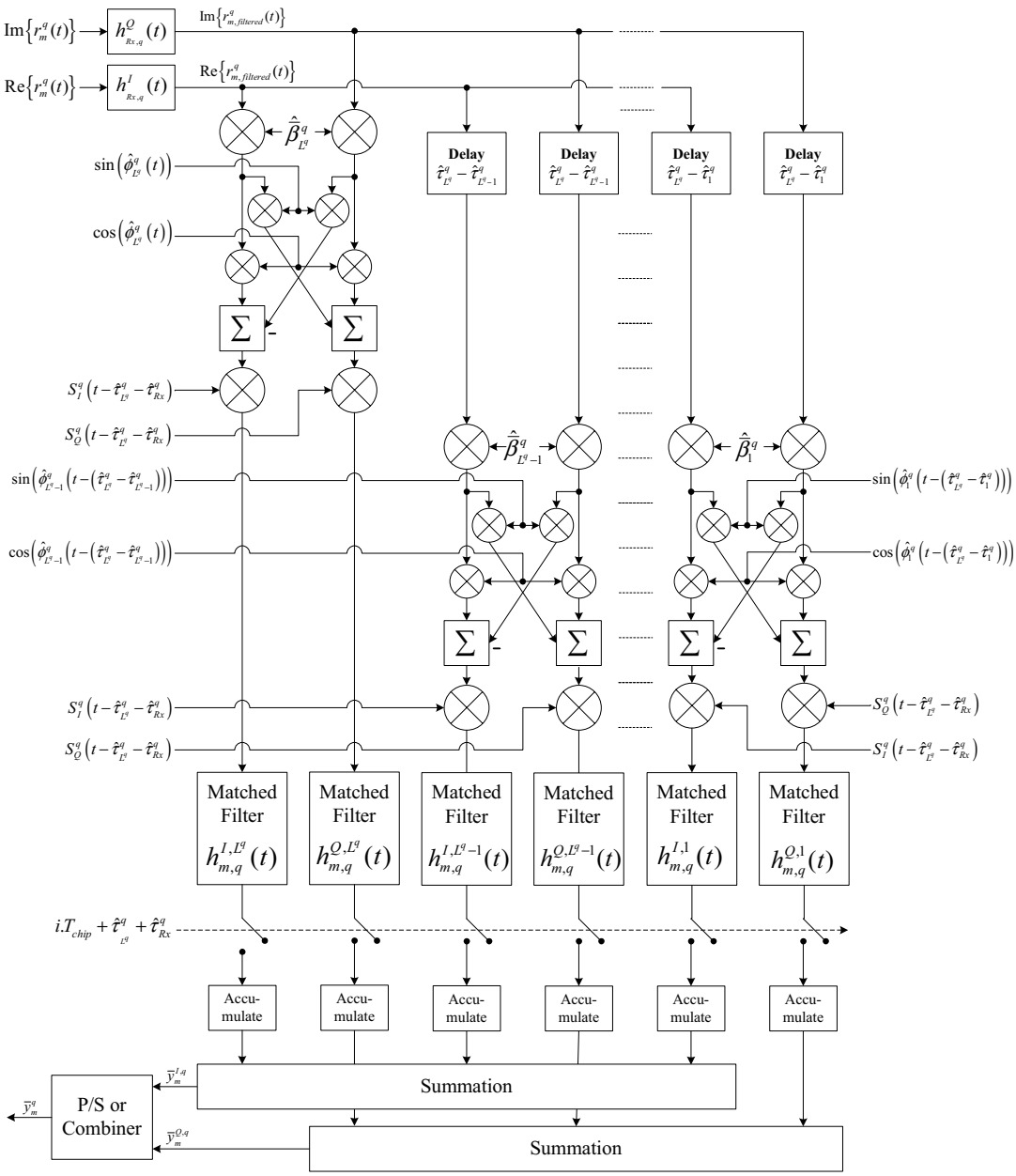

Figure 2: Complex DS/SSMA QPSK RAKE receiver structure

path delays, I-channel and Q-channel receive filter phase distortions and each of the multipath component's channel phase, i.e. $\hat{\phi}_i^q\left(t-(\hat{\tau}_{L^q}-\hat{\tau}_i^q)\right) = \phi_i^q\left(t-(\tau_{L^q}-\tau_i^q)\right)$, for $i = 1, 2, ..., L^q$.

In order to despread user-q's m^{th} complex received signal, each of the L^q phase corrected I-channel and Q-channel signals are respread with delayed versions of user-q's I-channel and Q-channel spreading sequences, $S_I^q\left(t-\hat{\tau}_{L^q}^q-\hat{\tau}_{Rx}^q\right)$ and $S_Q^q\left(t-\hat{\tau}_{L^q}^q-\hat{\tau}_{Rx}^q\right)$, respectively. The time delays $\hat{\tau}_{L^q}^q$ and $\hat{\tau}_{Rx}^q$ introduced into the spreading sequences are estimates of the total delay experienced by the realigned set of complex received signals and the time delay introduced by the receive filters, respectively. Despreading is completely successful only if the receiver has perfect knowledge of these time delays.

Continuing the demodulation procedure, the I-channel and Q-channel despread signals of the ith RAKE receiver tap are processed by the respective matched filters $h_{m,q}^{I,i}(t)$ and $h_{m,q}^{Q,i}(t)$. These filters are matched to the chip-level pulse shaping filters employed in the DS/SSMA QPSK transmitter. The outputs of the L^q I-channel and Q-channel matched filters are sampled at time instance

$$\begin{aligned}\overline{y}_{m,j}^{I,q} =& \frac{T_{chip}}{T_s}\sum_{i=1}^{L^q}\sum_{a=1}^{T_s/T_{chip}}\Big[\Big(\hat{\overline{\beta}}_i^q\Big[\mathrm{Re}\Big\{r_{m,filtered}^q\left(t-(\hat{\tau}_{L^q}^q-\hat{\tau}_i^q)\right)\Big\}.\cos\Big(\hat{\phi}_i^q\left(t-(\hat{\tau}_{L^q}-\hat{\tau}_i^q)\right)\Big)-\\ &\mathrm{Im}\Big\{r_{m,filtered}^q\left(t-(\hat{\tau}_{L^q}^q-\hat{\tau}_i^q)\right)\Big\}.\sin\Big(\hat{\phi}_i^q\left(t-(\hat{\tau}_{L^q}-\hat{\tau}_i^q)\right)\Big)\Big]\times\\ &S_I^q\left(t-\hat{\tau}_{L^q}^q-\hat{\tau}_{Rx}^q\right))\otimes h_{m,q}^{I,i}(t)\Big]_{t=j.T_s+a.T_{chip}+\hat{\tau}_{L^q}^q+\hat{\tau}_{Rx}^q}\end{aligned} \tag{14}$$

$$\begin{aligned}\overline{y}_{m,j}^{Q,q} =& \frac{T_{chip}}{T_s}\sum_{i=1}^{L^q}\sum_{a=1}^{T_s/T_{chip}}\Big[\Big(\hat{\overline{\beta}}_i^q\Big[\mathrm{Im}\Big\{r_{m,filtered}^q\left(t-(\hat{\tau}_{L^q}^q-\hat{\tau}_i^q)\right)\Big\}.\sin\Big(\hat{\phi}_i^q\left(t-(\hat{\tau}_{L^q}-\hat{\tau}_i^q)\right)\Big)+\\ &\mathrm{Re}\Big\{r_{m,filtered}^q\left(t-(\hat{\tau}_{L^q}^q-\hat{\tau}_i^q)\right)\Big\}.\cos\Big(\hat{\phi}_i^q\left(t-(\hat{\tau}_{L^q}-\hat{\tau}_i^q)\right)\Big)\Big]\times\\ &S_Q^q\left(t-\hat{\tau}_{L^q}^q-\hat{\tau}_{Rx}^q\right)\Big)\otimes h_{m,q}^{Q,i}(t)\Big]_{t=j.T_s+a.T_{chip}+\hat{\tau}_{L^q}^q+\hat{\tau}_{Rx}^q}\end{aligned} \tag{15}$$

$$\hat{\overline{\alpha}}_{m,j}^q = \frac{T_{chip}}{T_s}\sum_{i=1}^{L^q}\sum_{a=1}^{T_s/T_{chip}}\hat{\overline{\beta}}_i^q\left[\hat{\alpha}_i^q\left(t-(\hat{\tau}_{L^q}^q-\hat{\tau}_i^q)\right)\otimes h_{ave,q}^i(t)\right]_{t=j.T_s+a.T_{chip}+\hat{\tau}_{L^q}^q+\hat{\tau}_{Rx}^q} \tag{16}$$

$t = a.T_{chip} + \hat{\tau}_{L^q}^q + \hat{\tau}_{Rx}^q$, with T_{chip} the duration of a spreading sequence chip. Each of the I-channel and Q-channel matched filter outputs are accumulated for a duration of T_s [s], whereafter the accumulated values are normalised with respect to T_s/T_{chip}. The L^q I-channel and Q-channel accumulated values are then linearly combined to give estimates of the jth symbols in the original transmitted symbol vectors $\overline{c}_m^{I,q}$ and $\overline{c}_m^{Q,q}$, respectively. These symbol estimates for the I-channel and Q-channel are given by Equation (14) and Equation (15), respectively. Finalising the demodulation process, user-q's DS/SSMA QPSK RAKE receiver creates the output vector $\overline{y}_m^q$, which is an estimate of the original DS/SSMA QPSK transmitter input vector $\overline{c}_m^q$. This is accomplished by linearly combining the elements from $\overline{y}_m^{I,q}$ and $\overline{y}_m^{Q,q}$.

4.3 Average Output Fading Amplitude Calculation for Complex DS/SSMA QPSK Systems with RAKE Receivers

The first step in the calculation of user-q's average fading amplitude for the ith multipath fading channel component is to delay an estimate of its instantaneous fading amplitude $\hat{\alpha}_i^q(t)$ by $(\hat{\tau}_{L^q}^q - \hat{\tau}_i^q)$ [s]. Next, this delayed estimate of the ith channel component's instantaneous fading amplitude is filtered using an averaging filter $h_{ave,q}^i(t)$, which has an impulse response identical to the matched filters used in Figure 2. Recall that the delayed complex received signal $r_{m,filtered}^q(t-(\hat{\tau}_{L^q}^q-\hat{\tau}_i^q))$, with $i = 1, 2, ..., L^q$, is scaled by the average envelope amplitude estimate $\hat{\overline{\beta}}_i^q$ during MRC. Thus, the average fading amplitudes associated with the elements in receiver output vector $\overline{y}_m^q$ are normalised averages of the linear combination of the delayed average fading amplitudes experienced by each of the multipath components. Since the same data bits are transmitted on the I-channel and Q-channel, calculation of an estimate of the average fading amplitude associated with the jth element of user-q's receiver output vector $\overline{y}_m^q$, is accomplished using Equation (16) where $\hat{\overline{\beta}}_i^q$ and $\hat{\tau}_i^q$ are estimates of the ith multipath component's average envelope amplitude and delay, respectively.

5. COMPLEX MULTIPATH FADING CHANNEL SIMULATOR

The use of the Hilbert transform in a classic *Clarke* flat fading channel simulator can be negated by assuming that the ith multipath signal component transversing a multipath fading channel has already been decomposed into real and imaginary parts, i.e.:

$$u_i(t) = \mathrm{Re}\{u_i(t)\} + j.\,\mathrm{Im}\{u_i(t)\} \tag{17}$$

Now, define a complex fading flat fading process:

$$\begin{aligned}\varpi_i(t) =& \alpha_i(t).\cos(\phi_i(t)) +\\ & C_i^{LOS} + j.\alpha_i(t).\sin(\phi_i(t))\end{aligned} \tag{18}$$

where $\alpha_i(t)$ and $\phi_i(t)$ are the instantaneous fading amplitude and phase of the ith multipath component, respectively. The constant C_i^{LOS} dictates the Line-of-Sight (LOS) signal strength. It can easily be shown that the ith complex multipath fading channel component is given by:

$$b_i(t) = \mathrm{Re}\{b_i(t)\} + j.\,\mathrm{Im}\{b_i(t)\} = \varpi_i(t).u_i(t) \tag{19}$$

Thus, the in-phase and quadrature outputs of the ith flat fading channel, operating on a complex input signal, are given by:

$$\begin{aligned}\mathrm{Re}\{b_i(t)\} =& \mathrm{Re}\{\varpi_i(t)\}.\mathrm{Re}\{u_i(t)\} -\\ & \mathrm{Im}\{\varpi_i(t)\}.\mathrm{Im}\{u_i(t)\}\end{aligned} \tag{20}$$

and:

$$\begin{aligned}\mathrm{Im}\{b_i(t)\} =& \mathrm{Re}\{\varpi_i(t)\}.\mathrm{Im}\{u_i(t)\} +\\ & \mathrm{Im}\{\varpi_i(t)\}.\mathrm{Re}\{u_i(t)\}\end{aligned} \tag{21}$$

respectively.

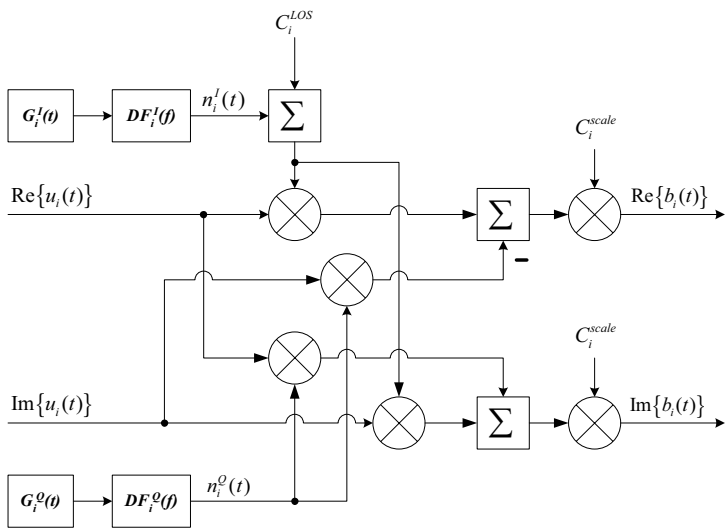

Figure 3: Complex flat fading channel simulator, based on *Clarke's* model

Figure 3 shows a simple complex implementation of the *Clarke*'s flat fading channel that realises Equation (20) and Equation (21). From this figure it is clear that:

$$\mathrm{Re}\{b_i(t)\} = C_i^{scale}\left[\left(n_i^I(t) + C_i^{LOS}\right).\mathrm{Re}\{u_i(t)\} - n_i^Q(t).\mathrm{Im}\{u_i(t)\}\right] \tag{22}$$

and:

$$\mathrm{Im}\{b_i(t)\} = C_i^{scale}\left[\left(n_i^I(t) + C_i^{LOS}\right).\mathrm{Im}\{u_i(t)\} + n_i^Q(t).\mathrm{Re}\{u_i(t)\}\right] \tag{23}$$

where $n_i^I(t)$ and $n_i^Q(t)$ are the respective outputs of Doppler filters $DF_i^I(f)$ and $DF_i^Q(f)$ for Gaussian input signals. The constant C_i^{scale} is chosen such that the channel simulator input signal power and output signal power are equal in magnitude, resulting in the following expression:

$$C_i^{scale} = \frac{1}{\sqrt{2 + \left(C_i^{LOS}\right)^2}} \tag{24}$$

Furthermore, it can be shown that the Rician factor for the complex flat fading channel simulator is given by:

$$K_i = 20\log_{10}\left(\frac{C_i^{LOS}}{\sqrt{2}}\right) \tag{25}$$

Figure 4 shows an L-path complex multipath fading channel simulator, constructed using L distinct complex flat fading channel simulators, denoted by blocks $Complex\,FFCS_1$ to $Complex\,FFCS_L$. The simulator functions as follows: Firstly, an appropriate L-path power delay profile is chosen. L time-delayed versions of the transmitted signal are then created by using a L-tap delay line with delay times equal to that of the required power delay profile. Next, the time delayed signal $a_i(t)$, with $i = 1, 2, ..., L$, is scaled by the factor $\overline{\beta}_i$, which represents the average amplitude of the ith multipath component, as specified by the power delay profile. These delayed and scaled signals are then processed by L unique flat fading channel simulators, such as the one shown in Figure 3. Thus, it is possible to define a unique maximum Doppler frequency and Rician factor for each multipath component. The resultant outputs of the flat fading channel simulators, denoted as $b_i(t)$, with $i = 1, 2, 3, ..., L$, are then added to give the frequency selective fading channel simulator's complex output signal $r(t)$.

6. PERFORMANCE EVALUATION PLATFORM

Figure 5 depicts the complete frequency selective fading channel simulation platform used in this study. This platform is built around the RAKE receiver-based complex DS/SSMA QPSK communication system discussed in part I of this paper. Table 1 summarises the general wideband transmitter configuration supported by each of the users in the CDMA environment. As indicated by this table, the BER performances of coded wideband systems employing either unfiltered, or filtered CSS families were investigated: With unfiltered CSS families, such as the ZC and QPH families considered in this study, there is no bandlimiting built into the CSSs. Thus, additional pulse shaping is required to ensure effective spectrum utilisation. In this study chip-level square-root Nyquist pulse shaping was employed.

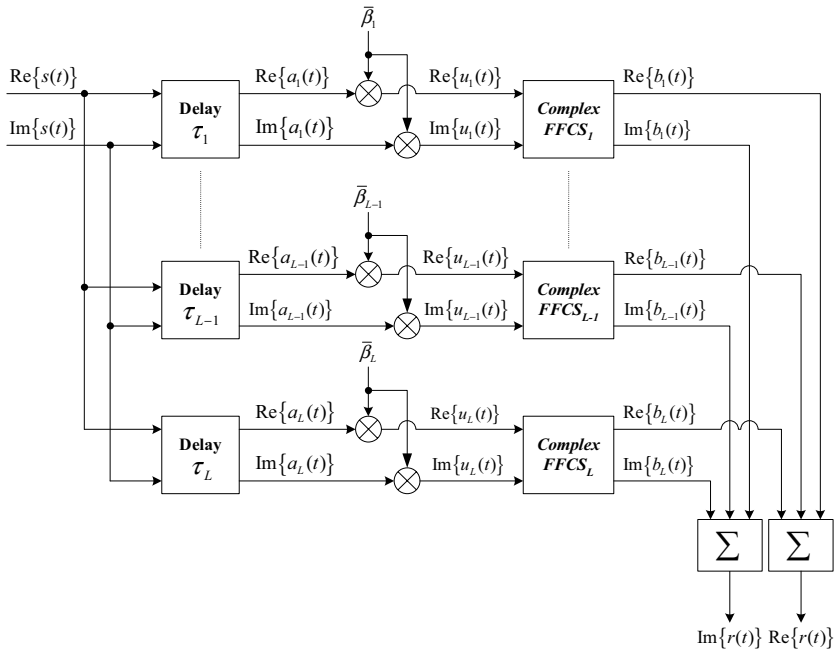

Figure 4: Complex multipath fading channel simulator

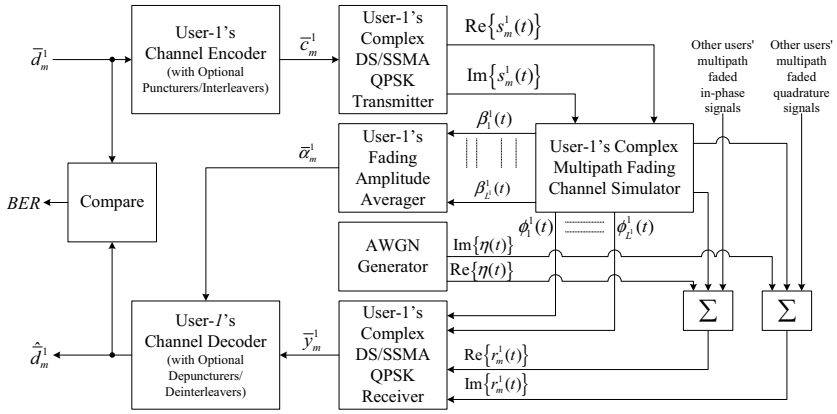

Figure 5: General multipath fading channel simulator platform

In the case of the filtered ABC and DSB CE-LI-RU filtered GCL CSS, no additional bandlimiting is required, i.e. simple rectangular pulse shaping is used. It has been shown that, when the spreading sequence length M_{seq} is sufficiently large, the *linearly interpolating root-of-unity* filtering technique [4, 14] employed in the generation of a DSB CE-LI-RU filtered GCL CSS produces a signal bandwidth equivalent to that generated by Nyquist filtering with a roll-off factor approaching $\varsigma = 0$.

Up to 10 distinct CDMA users are supported by the simulation platform depicted in Figure 5. For each of the 10 possible users in the CDMA system a unique complex multipath fading channel simulator configuration was chosen, since the movement of the users' wideband complex transmitters relative to the single complex RAKE receiver is stochastic. Perfect power control was assumed, i.e. the average powers of all the users' corrupted signals entering user-1's RAKE receiver are equal. Listed in Table 2 and Table 3 are the complex multipath fading channel simulator configurations for the 10 possible users. Each user's multipath fading channel simulator were configured to have 3 statistically independent paths. The Rician factor and Doppler spreading for the ith path of each user's channel simulator, respectively denoted as K_i and $B_{D,i}$, were chosen randomly. Each user's path powers and relative path delays, respectively denoted as τ_i and P_i, with $i = 1, 2, 3$, were chosen according to exponentially decaying power delay profiles that conform to the requirements for frequency selective fading. Note

		User Number				
		1	2	3	4	5
Path 1 Setup	P_1 [dB]	-0.1394	-0.3866	-0.2820	-0.5303	-1.0279
	$K_1[dB]$	9	9	9	9	9
	$B_{D,1}$ [Hz]	100	33	67	33	100
	τ_1 [μs]	0	20	30	10	40
Path 2 Setup	P_2 [dB]	-15.1394	-10.8866	-12.2820	-9.5303	-7.0279
	K_2 [dB]	0	0	0	0	0
	$B_{D,2}$ [Hz]	67	100	33	67	33
	τ_2 [μs]	100	90	110	70	80
Path 3 Setup	P_3 [dB]	-30.1394	-24.3866	-24.2820	-24.5303	-19.0279
	K_3 [dB]	-100	-100	-100	-100	-100
	$B_{D,3}$ [Hz]	33	67	100	100	67
	τ_3 [μs]	200	180	190	170	160

Table 2: Complex multipath fading channel simulator configurations for users 1 to 5

		User Number				
		6	7	8	9	10
Path 1 Setup	P_1 [dB]	-0.3820	-0.2131	-0.3764	-0.2063	-0.5303
	$K_1[dB]$	9	9	9	9	9
	$B_{D,1}$ [Hz]	67	100	67	33	33
	τ_1 [μs]	20	30	10	0	30
Path 2 Setup	P_2 [dB]	-10.8820	-13.7131	-10.8764	-13.7063	-9.5303
	K_2 [dB]	0	0	0	0	0
	$B_{D,2}$ [Hz]	100	100	67	33	67
	τ_2 [μs]	90	120	80	90	90
Path 3 Setup	P_3 [dB]	-25.8820	-22.7131	-28.8764	-24.2063	-24.5303
	K_3 [dB]	-100	-100	-100	-100	-100
	$B_{D,3}$ [Hz]	33	67	33	67	33
	τ_3 [μs]	190	180	200	160	190

Table 3: Complex multipath fading channel simulator configurations for users 6 to 10

Configuration Parameter	Setting
Unspread Symbol Rate	1000 [symbols/s]
CSS Length	63 [chips]
CSS Rate	63000 [chips/s]
Effective RF Carrier Frequency	900 [MHz]
Pulse Shaping Filters: Unfiltered CSSs	Shaping: Square-Root Nyquist Roll-off Factor: $\varsigma = 0.5$
Pulse Shaping Filters: Filtered CSSs	Shaping: Rectangular Roll-off Factor: N/A
Power Control	Perfect
CSS Families Supported	ABC, DSB CE-LI-RU Filtered GCL, Unfiltered ZC, Unfiltered QPH

Table 1: Wideband complex DS/SSMA QPSK transmitter configuration

that the maximum access delay of user-1 is $\tau_{max} = 200$ μs, which is 12.6 CSS chips, or one fifth of a CSS in duration.

Table 4 details the complex DS/SSMA QPSK RAKE receiver's general configuration. The single RAKE receiver present in the CDMA system was configured to be perfectly synchronised with the received signal initially generated by user-1's wideband complex transmitter, i.e. perfect carrier, chip and symbol synchronisation were assumed on each of the RAKE taps.

7. SIMULATION RESULTS

The uncoded and VA decoded RS block code BER performance results presented in the following two subsections were obtained using the performance evaluation platform shown in Figure 5. The transmitter and receiver structures of the users in the CDMA system were configured according to Table 1 and Table 4, respectively. Each user's complex multipath fading channel simulator was configured uniquely according to Table 2 and Table 3.

The performance evaluation platform was implemented in C++ using Object Orientated Programming (OOP) approach. The C++ code was compiled using *Intel*'s *ICC* and *GNU*'s *G++* compilers for *Linux* platforms. The BER

Configuration Parameter	Setting
Unspread Symbol Rate	1000 [symbols/s]
CSS Length	63 [chips]
CSS Rate	63000 [chips/s]
Effective RF Carrier Frequency	900 [MHz]
Receive Filters	6th Order Elliptic
Matched Filters: Unfiltered CSSs	Shaping: Square-Root Nyquist Roll-off Factor: $\varsigma = 0.5$
Matched Filters: Filtered CSSs	Shaping: Rectangular Roll-off Factor: N/A
RAKE Receiver Configuration	Perfect MRC
Symbol Synchronisation	Perfect for Each RAKE Tap
Carrier Synchronisation	Perfect for Each RAKE Tap
Code Lock	Perfect for Each RAKE Tap
CSS Families Supported	ABC, DSB CE-LI-RU Filtered GCL, Unfiltered ZC, Unfiltered QPH

Table 4: Wideband complex DS/SSMA QPSK RAKE receiver configuration

performance results presented in *Section* 3 were obtained in record breaking time by distributing the processor load of the simulation software over the multiple workstations in the *University of Pretoria*'s *I-percube*, donated by *Intel*. The *I-percube* consists of 16 2.4GHz *Pentium 4* stations, each station running a *Mandrake Linux* operating system. The 16 stations are interconnected via *Fast Ethernet* connections. Process migration and message handling between the stations are managed transparently by *Open Mosix* for *Linux*.

7.1 Uncoded Results

In Figure 6, Figure 7, Figure 8 and Figure 9 the simulated BER performances curves are presented for uncoded single user, 5-user and 10-user DS/SSMA systems employing ABC, DSB CE-LI-RU filtered GCL, QPH and ZC CSSs, respectively. Both RAKE and classic (1-tap RAKE) receivers were considered. From these figures the following important observations can be made:

- The 3-tap RAKE receivers show improved BER performances when compared to the classic non-RAKE receivers, as was to be expected. The performance improvement is most noticeable with ZC sequences. This is due to these CSSs' superior cross-correlation properties [6], resulting in low self-noise levels in the RAKE receivers.
- As the number of users in the system increases, the MUI becomes more severe. From the figures it is clear that ABC sequences suffer the most from MUI, due to their poor cross-correlation properties [6].

7.2 VA Decoded RS Code Results

Figure 10, Figure 11, Figure 12 and Figure 13 present simulated BER performance results for $(7, 5, 3)$ RS block

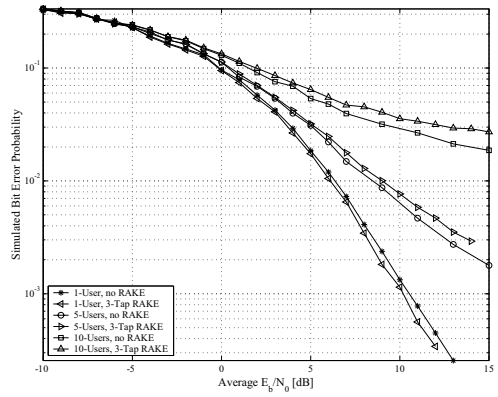

Figure 6: Uncoded system employing ABC CSSs

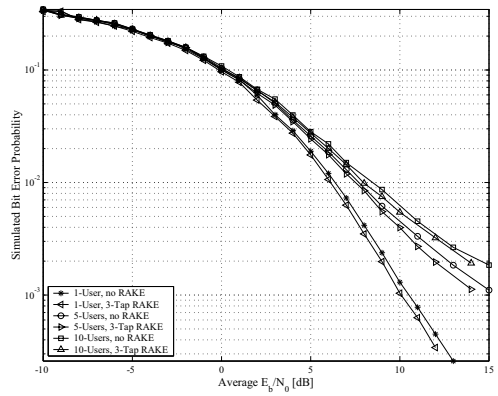

Figure 7: Uncoded system employing DSB CE-LI-RU filtered GCL CSSs

coded (with message and codeword symbols from Galois field $GF\left(2^3\right)$) single user, 5-user and 10-user DS/SSMA systems employing ABC, DSB CE-LI-RU filtered GCL, QPH and ZC CSSs, respectively. From these results the following important observations can be drawn:

- The RS coded systems show marked BER improvements, especially for the 10-user scenarios. By introducing the $(7, 5, 3)$ RS block codes, coding diversity has been introduced into the system, resulting in better MUI suppression. ABC sequences, however, still performed poorly due to their weak cross-correlation characteristics.
- The systems employing unfiltered ZC CSSs once again performed the best.
- Including CSI into the VA decoders' branch metric calculations delivered unimpressive performance improvements of no more than 0.4 dB in the single user scenarios, and even less for more users.

8. CONCLUSIONS

This paper presented a simulation study of a RAKE receiver-based DS/SSMA communication system employ-

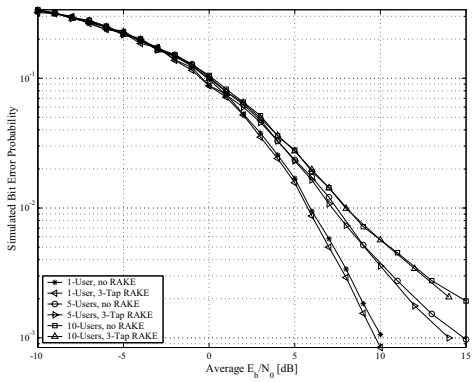

Figure 8: Uncoded system employing QPH CSSs

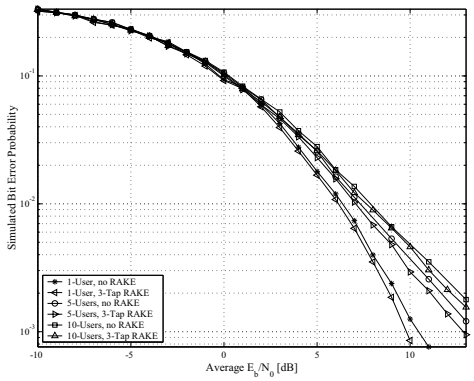

Figure 9: Uncoded system employing ZC CSSs

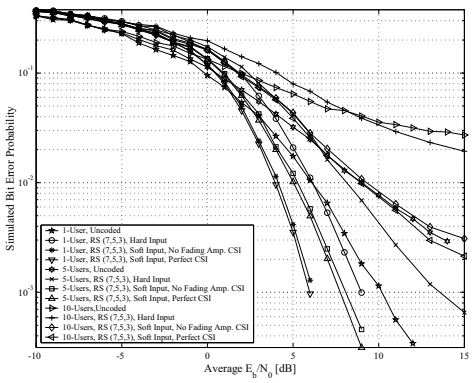

Figure 10: (7, 5, 3) RS coded system employing ABC ZC CSSs

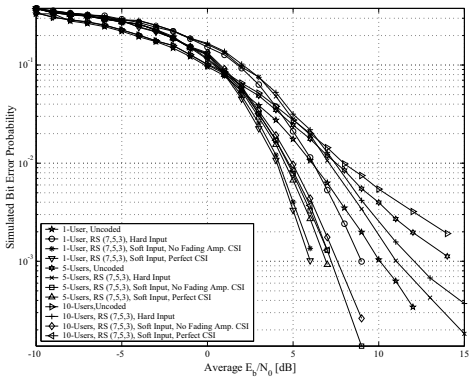

Figure 11: (7, 5, 3) RS coded system employing DSB CE-LI-RU filtered GCL CSSs

ing VA decoded RS block codes and CSSs, operating in multi-user, multipath fading channel conditions. It commenced with background information on the VA decoding of linear block codes, as well as a discussion of the filtered and unfiltered CSS families considered in this study. Simple complex DS/SSMA QPSK transmitter and RAKE receiver simulation models, capable of replicating the operation of a realistic multi-user DS/SSMA communication system, without requiring actual carriers or high sampling frequencies, were also considered. A novel complex multipath fading channel simulator model, constructed using complex *Clarke*-like flat fading channel simulators, was presented. The complex RAKE receiver-based DS/SSMA QPSK communication system simulation structures, as well as the novel complex multipath fading channel simulator model was then used to construct a versatile performance evaluation platform, which was used to obtain this study's simulated BER performance curves for VA decoded nonbinary RS blocks in multi-user, multipath fading channel conditions. The simulation results obtained during this study showed that the VA can be used as effective ML block code decoder for RS block codes in multipath, multi-user channel conditions. Further, it was shown that, in terms of MUI, the unfiltered QPH CSSs were the most optimal CSS family considered, whereas ABC CSSs were the least optimal. Lastly, it was shown that the complexity of using CSI in the VA decoding process does not justify the potential increase in BER performance.

9. ACKNOWLEDGEMENTS

The authors wish to thank *Intel* for its donation of the *I-percube* to the *University of Pretoria*, as well as *Paul Greeff* and *Jan Gütter* for their invaluable knowledge on the usage of thereof as efficient and powerful simulation tool.

REFERENCES

[1] L. R. Bahl, J. Cocke, F. Jelinek, and J. Raviv, "Optimal Decoding of Linear Codes for Minimizing Symbol Error Rate," *IEEE Transactions on Information Theory*, pp. 284–287, March 1974.

[2] J. Wolf, "Ef.cient Maximum Likelihood Decoding of Linear Block Codes Using a Trellis," *IEEE Transactions on Information Theory*, vol. IT24, pp. 76–80, January 1978.

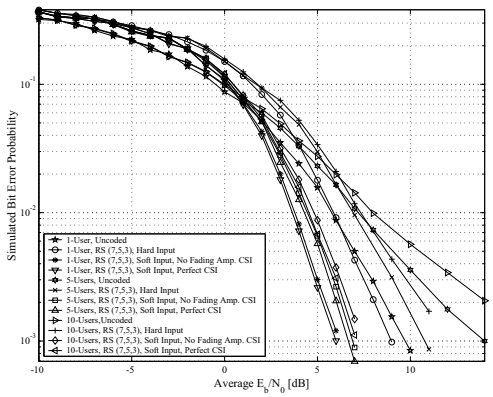

Figure 12: (7, 5, 3) RS coded system employing QPH CSSs

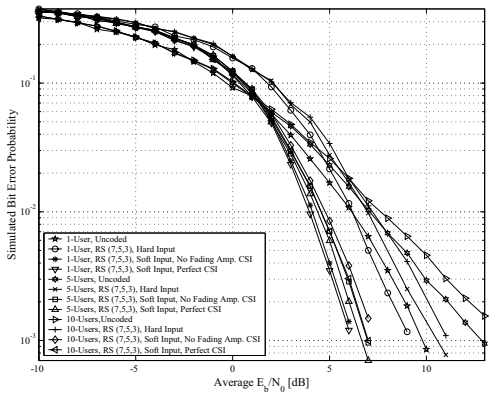

Figure 11: (7, 5, 3) RS coded system employing ZC CSSs

[3] J. Hagenauer, "Viterbi Decoding of Convolutional Codes for Fading and Burst Channels," in *Proc., Int. Zurich Seminar on Digital Communications*, (Zurich, Switzerland), pp. G2.1–G2.7, 1980.

[4] M. P. Lötter and L. P. Linde, "Constant Envelope Filtering of Complex Spreading Sequences," *IEEE Electronics Letters*, vol. 31, no. 17, pp. 1406–1407, 17 August 1995.

[5] M. P. Lötter and L. P. Linde, "A Class of Bandlimited Complex Spreading Sequences with Analytic Properties," in Proc., *IEEE Int. Symp. on Spread Spectrum Techniques and Applications*, (Mainz, Germany), pp. 662–666, 2225 September 1996.

[6] M. Jamil, L. P. Linde, J. E. Cilliers, and D. J. van Wyk, "Comparison of Complex Spreading Sequences Based on Filtering Methods and Mean Square Correlation Characteristics," *Transactions of the SAIEE*, vol. 89, no. 3, pp. 98–112, September 1998.

[7] J. G. Proakis, *Digital Communications. New York*, NY, USA: McGrawHill, Third ed., 1995.

[8] C. Heegard and S. B. Wicker, *Turbo Coding*. Norwell, MA, USA: Kluwer Academic Publishers, First ed., 1999.

[9] L. Staphorst and L. P. Linde, "On the Viterbi Decoding of Linear Block Codes," *Transactions of the SAIEE*, vol. 94, no. 4, pp. 28–41, December 2003.

[10] B. M. Popović, "Generalized Chirp-like Polyphase Sequences with Optimum Correlation Properties," *IEEE Transactions on Information Theory*, vol. 38, July 1992.

[11] R. L. Frank and S. A. Zadoff, "Phase Shift Pulse Codes with Good Periodic Correlation Properties," IRE Transactions on Information Theory, vol. IT-7, pp. 381–382, October 1962.

[12] S. M. Korne and D. V. Sarwate, "Quadriphase Sequences for Spread Spectrum Multiple Access Communication," *IEEE Transactions on Information Theory*, vol. IT38, no. 3, pp. 1101–1113, May 1992.

[13] M. Jamil, "Comparative Study of Complex Spreading Sequences for CDMA Applications," Master's thesis, University of Pretoria, May 1999.

[14] M. P. Lötter, "A Generalised Linear Root-of-Unity Interpolation Filter," in *Proc., IEEE COMSIG'95*, (University of Pretoria, Pretoria, South Africa), pp. 43–46, September 1995.

[15] L. Staphorst, M. Jamil, and L. P. Linde, "Performance of a Synchronous Balanced QPSK CDMA System Using Complex Spreading Sequences in AWGN," in *Proc., IEEE AFRICON'99*, (Cape Town, South Africa), pp. 215–220, 28 September - 1 October 1999.

[16] L. Staphorst, M. Jamil, and L. P. Linde, "Performance Evaluation of a QPSK System Employing Complex Spreading Sequences in a Fading Environment," in *Proc., IEEE VTC'99-Fall*, (Asterdam, The Netherlands), pp. 2964–2967, 1922 September 1999.

[17] IS-95 Interim Standard: *'An Overview of the Application of Code Division Multiple Access (CDMA) to Digital Cellular Systems and Personal Cellular Networks'*, Qualcomm Inc., May 1992.

[18] E. Biglieri, "Coding and Modulation for the Fading Channels." Presented at ISSSTA'98, Tutorial 4, 24 September 1998.